Boundary Treatment for a Cartesian Grid Method

Boundary Treatment for a Cartesian Grid Method

H. Forrer

Research Report No. 96-04
April 1996

Seminar für Angewandte Mathematik
Eidgenössische Technische Hochschule
CH-8092 Zürich
Switzerland

Boundary Treatment for a Cartesian Grid Method

H. Forrer

Seminar für Angewandte Mathematik
Eidgenössische Technische Hochschule
CH-8092 Zürich
Switzerland

Research Report No. 96-04 April 1996

Abstract

We are interested in a numerical solution to the Euler Equations in complicated 2-dimensional geometries using a Cartesian grid method. To avoid stability problems or loss of accuracy along the boundary, this requires a special treatment of the irregular cells along the boundary.
In this paper we present a new technique for the boundary treatment. The technique is built upon a high resolution finite volume method with dimensional splitting. To avoid stability problems for small boundary cells due to instable fluxes, we use an enlargement of the domain of dependence. The enlarged domains may lie beyond the boundary. By a local mirroring at the boundary we determine values of the flow variables also for these regions. This enables us to calculate stable fluxes for the small boundary cells. These fluxes are formally of second order accuracy.
Among other examples we calculate a Prandtl-Meyer expansion, a double Mach reflection and a shock diffraction by a pair of cylinders. The latter example points to a major advantage of Cartesian grid methods, the ability to cope with complicated geometries.

1 Introduction

Consider the Euler Equations in two space dimensions, a system of hyperbolic partial differential equations:

$$U_t + F_x + G_y = 0, \tag{1}$$

$$U = \begin{pmatrix} \rho \\ \rho u \\ \rho v \\ \rho e \end{pmatrix}, \quad F = \begin{pmatrix} \rho u \\ \rho u^2 + p \\ \rho uv \\ u(\rho e + p) \end{pmatrix}, \quad G = \begin{pmatrix} \rho v \\ \rho uv \\ \rho v^2 + p \\ v(\rho e + p) \end{pmatrix},$$

$$p = (\gamma - 1)(\rho e - \frac{1}{2}\rho(u^2 + v^2)).$$

Where ρ is the mass density, $(u, v)^T$ the velocity vector, e the energy density, p the pressure and $\gamma = 1.4$. These equations (1) describe inviscid compressible flows. We are interested in such a flow field about some arbitrary body. Therefore we need a discretization of the space. The method should be built upon existing finite volume methods. For the discretization we use a Cartesian grid. To do this, let h be a grid parameter and set the points (x_i, y_j) as $x_i = x_0 + h \cdot i, \quad y_j = y_0 + h \cdot j, \quad i, j \in \mathbb{Z}$. The regular grid cell C_{ij} is then given by:

$$C_{ij} = [x_i, x_{i+1}] \times [y_j, y_{j+1}].$$

A given body cuts some cells out of the grid completely or partially. We assume that h is so small that the boundary of the body intersects with the boundary of each cell only in at most two points. We modify such a cell with two intersection points by connecting these two points by a straight line (cf. Figure 1).

By this discretization close to the body triangles, quadrangles and pentagons arise, denoted with C_{ij} as well, having areas $|C_{ij}|$, which can get very small.

Let the vector U_{ij}^n be a weighted mean over the cell C_{ij} of the exact solution $U = (\rho, \rho u, \rho v, \rho e)^T$ of the differential equation (1) at time t_n:

$$U_{ij}^n \approx \frac{1}{|C_{ij}|} \int_{C_{ij}} U(x, y, t_n) dx\, dy. \tag{2}$$

An advantage of Cartesian grid methods is that one can use existing fast high resolution methods, e.g. the ones used in CLAWPACK of LeVeque *, with an extension of a special treatment for the boundary cells C_{ij}. It is the aim of this paper to present a second order treatment of these boundary cells.

An other advantage is that flows about very complicated geometries can by calculated without to much cost in the grid generation. But it is still an open question,

*available by anonymous ftp from amath.washington.edu in the directory pub/leveque/programs/clawpack

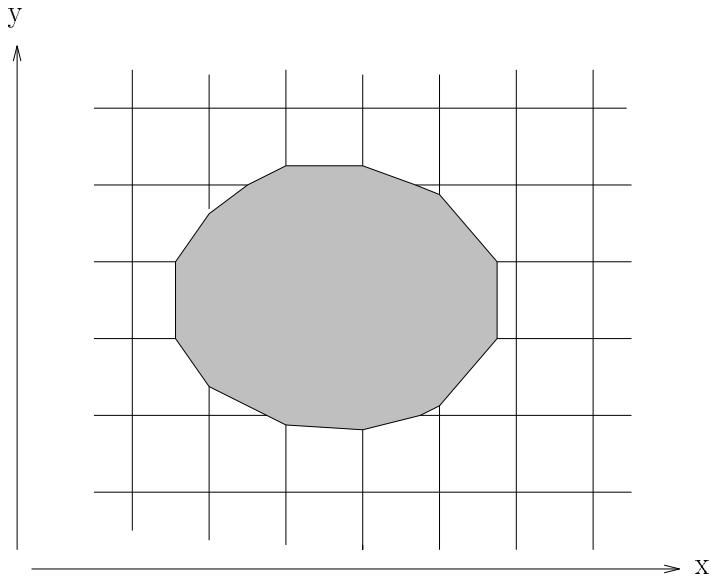

Figure 1: Discretization of the space around some body.

whether one should prefer body-fitted grids or Cartesian grids for a calculation of the full Navier-Stokes Equations.

Now we describe the main ideas of two different boundary treatments. Berger and LeVeque [1] use the following standard conservative finite volume method:

$$U_{ij}^{n+1} = U_{ij}^{n} + \frac{\Delta t}{h}(F_{ij}^{n} - F_{i+1,j}^{n} + G_{ij}^{n} - G_{i,j+1}^{n}). \tag{3}$$

The fluxes F_{ij}^{n} are obtained by solving a Riemann problem:

$$F_{ij}^{n} = F(U^{*}(U_{i-1,j}^{n}, U_{ij}^{n})), \tag{4}$$

where U^{*} is the solution of the Riemann problem for the equation $U_t + F_x = 0$ with initial values $U_{i-1,j}^{n}$ and U_{ij}^{n} at the location $\frac{x}{t} = 0$. G_{ij}^{n} is obtained analogously. Second order is achieved by adding a correction term to the fluxes, which needs limited gradients.

For the boundary cells they generalize the method as follows:

$$U_{ij}^{n+1} = U_{ij}^{n} + \frac{\Delta t}{|C_{ij}|}(F_{ij}^{n}\, ly_{ij} - F_{i+1,j}^{n}\, ly_{i+1,j} + G_{ij}^{n}\, lx_{ij} - G_{i,j+1}^{n}\, lx_{i,j+1} + H_{ij}^{n}\, l_{ij}). \tag{5}$$

Here H_{ij}^{n} denotes the flux along the boundary of the body. In (5) lx_{ij}, ly_{ij} and l_{ij} are the lengths of the straight lines around the boundary cell. For the boundary cell C_{ij} in Figure 2, we have: $lx_{ij} = |\Gamma_1|$, $ly_{ij} = |\Gamma_5|$, $lx_{i,j+1} = |\Gamma_4|$, $ly_{i+1,j} = |\Gamma_3|$, $l_{ij} = |\Gamma_2|$.

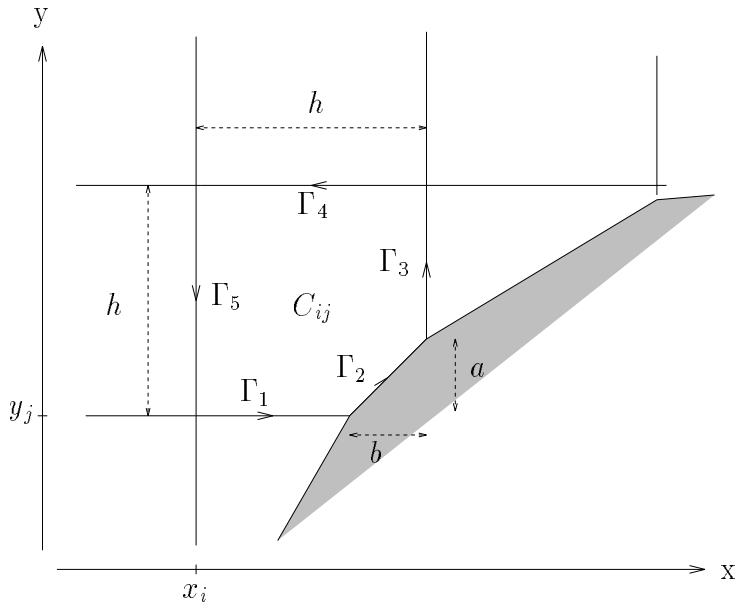

Figure 2: Boundary cell near the body.

The fluxes F_{ij}^n, G_{ij}^n and H_{ij}^n are now determined such that the method stays stable with a time step Δt which satisfies the CFL-condition for the regular cells.

The flux H_{ij}^n is obtained by solving a rotated Riemann problem for the equation

$$U_t + \frac{\partial}{\partial n}(\vec{n} \cdot (F, G)) = 0 \tag{6}$$

at the location of the cell interface to the body. $\frac{\partial}{\partial n}$ is the normal derivative in the direction of $\vec{n}$, the normal vector on the body boundary into the domain. Initial values of the Riemann problem are

$$U_b \quad \text{and} \quad R_{ij}(U_b). \tag{7}$$

The state U_b is obtained by a weighted mean over the auxiliary cell on Figure 3a). The operator $R_{ij}(.)$ is defined by a change of sign of the normal component of the velocity and by an identity in the tangential component, the density and the energy. So the state $R_{ij}(U)$ is obtained by mirroring the state U_b at the body boundary segment of the cell C_{ij}. With the solution of the rotated Riemann problem $U^*(R_{ij}(U_b), U_b)$ at the location of the interface of the cell and the body, H_{ij}^n is obtained by:

$$H_{ij}^n = \vec{n} \cdot (F(U^*), G(U^*)). \tag{8}$$

To calculate the fluxes F_{ij}^n, G_{ij}^n near the boundary, they solve two rotated Riemann problems orthogonally and tangentially to the wall with initial values as the weighted means over the auxiliary cells in Figure 3b/c. In case of an auxiliary cell

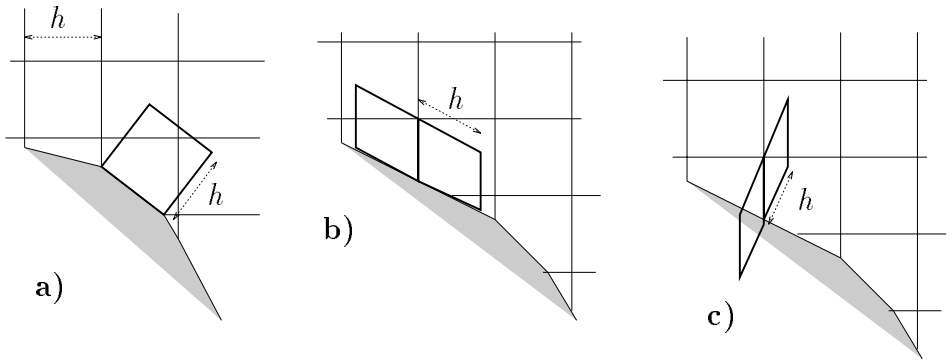

Figure 3: Auxiliary cells for the initial values of the rotated Riemann problems.

standing into the body (e.g. on Figure 3c), the value $R(U_b)$ of the calculation of an H-flux is needed there for the weighted mean. By solving the two rotated Riemann problems, they get numerical values for the tangential and the orthogonal fluxes $F^n_{\parallel}$ and $F^n_{\perp}$, by which F^n_{ij} and G^n_{ij} can be obtained.

This procedure of calculating the two orthogonal fluxes $F^n_{\parallel}$ and $F^n_{\perp}$ was introduced to guarantee cancellation of fluxes for very small boundary cells and so the method stays stable. The method is conservative as the flux H^n_{ij} is zero in the density, the tangential momentum and the energy component. In [2] they achieved no second order along the boundary. The method is known as h-box method.

An other Cartesian grid method is described by Pember et al. in [3]. There for the regular cells, the method looks formally the same as in (3). But the fluxes F^n_{ij} and G^n_{ij} are calculated differently. First for every cell limited gradients are defined, which are used to calculate time centered states $U^E_{ij}, U^W_{ij}, U^S_{ij}$ and U^N_{ij} in the middle of the cell interfaces. The flux F^n_{ij} is then obtained by solving a Riemann problem analogously to (4):

$$F^n_{ij} = F(U^*(U^E_{i-1,j}, U^W_{ij})). \tag{9}$$

The boundary treatment works in two steps:

1. For the grid cells close to the boundary on both sides of the boundary, weighted mean states U^{ext}_{ij} are calculated before every step (3):

$$U^{ext}_{ij} = \frac{\sum_{k,l=i-1,j-1}^{i+1,j+1} |C_{kl}| U_{kl}}{\sum_{k,l=i-1,j-1}^{i+1,j+1} |C_{kl}|} \tag{10}$$

   By this calculation we get weighted mean values for all cells near the boundary, and we can proceed as in step (3). The new states are denoted with $U^{n,ref}_{ij}$ near the boundary. This step is non conservative but stable.

2. To get from $U_{ij}^{n,ref}$ to a conservative U_{ij}^{n+1} for the cells along the boundary, a stable correction term is calculated by the construction of a flux H_{ij}^n (similarly as in (8)).

Because of its simplicity, this method was also used for calculations in three space dimensions.

A further Cartesian grid method is from Quirk [4], where boundary cells C_{ij} with areas $|C_{ij}| < \frac{1}{2}h^2$ are joined to suitable neighbor cells. This procedure leads to a loss in accuracy along the boundary.

These three methods are not of second order accuracy along the boundary. All of them were combined with the adaptive mesh refinement code (AMR) of Berger and Colella [5].

2 A new treatment for the small boundary cells

The various Cartesian grid methods often rely on dimensional splitting. Dimensional splitting is a special case of the Strang splitting [6]. Using dimensional splitting for the equation $u_t + Au_x + Bu_y = 0, u \in \mathbb{R}^n, \quad A, B \in \mathbb{R}^{n\times n}$ combines second order methods for the equations $u_t + Au_x = 0$ and $u_t + Bu_y = 0$ and yields a second order method for the whole equation as described below. These methods have the advantage of being economical in storage space and of being stable with a time step with CFL number 1.0. Thus dimensional splitting methods are efficient with respect to CPU time. As a disadvantage, one can object that the directions of the splitting along the two coordinate axes are not selected by the flow field. A standard dimensional splitting method can be built using the CLAWPACK package (cf. previous section), where for solving the one dimensional equation $u_t+F(u)_x = 0$, a Roe solver [7] is applied with an extension for sonic rarefaction waves (entropy fix [8] pp. 151-153). We used this method to test our new boundary treatment, which is similar to the h-box method of Berger and LeVeque [1] described in the previous section.

Using a dimensional splitting for the regular cells, we propagate the solution U_{ij}^n at time t_n into the solution U_{ij}^{n+1} at time $t_n + \Delta t$ by the following three steps:

$$\begin{aligned} U_{ij}^{n+\frac{1}{4}} &= U_{ij}^n + \tfrac{\Delta t}{2h}(F_{ij}^n - F_{i+1,j}^n) \\ U_{ij}^{n+\frac{3}{4}} &= U_{ij}^{n+\frac{1}{4}} + \tfrac{\Delta t}{h}(G_{ij}^{n+\frac{1}{4}} - G_{i,j+1}^{n+\frac{1}{4}}) \\ U_{ij}^{n+1} &= U_{ij}^{n+\frac{3}{4}} + \tfrac{\Delta t}{2h}(F_{ij}^{n+\frac{3}{4}} - F_{i+1,j}^{n+\frac{3}{4}}). \end{aligned} \tag{11}$$

$F_{ij}^n(U_{i-1,j}^n, U_{ij}^n)$ and $F_{ij}^{n+\frac{3}{4}}(U_{i-1,j}^{n+\frac{3}{4}}, U_{ij}^{n+\frac{3}{4}})$ are obtained as in (4) by solving a one dimensional Riemann problem. $G_{ij}^{n+\frac{1}{4}}$ is defined analogously by:

$$G_{ij}^{n+\frac{1}{4}} = G\left(U^*(U_{i,j-1}^{n+\frac{1}{4}}, U_{ij}^{n+\frac{1}{4}})\right), \tag{12}$$

where $U^*(.,.)$ is the solution of a Riemann problem for the equation $U_t + G(U)_y = 0$ at the location $\frac{y}{t} = 0$. The method (11) is stable with a time step

$$\Delta t \cdot \max(|\vec{u}| + c) < h\,,\ c = \sqrt{\gamma \frac{p}{\rho}} \text{ is the speed of sound.} \tag{13}$$

If the single steps in (11) are of second order accuracy, the total step $U_{ij}^n \mapsto U_{ij}^{n+1}$ is of second order accuracy. For a longer calculation, the integration by half a time step in (11) has only to be done at the beginning and at the end of the calculation because else they can be combined to an integration by full time step within second order accuracy.

For a boundary treatment based on dimensional splitting, one has to define numerical fluxes $F(\Gamma), G(\Gamma)$ along all the boundary segments Γ of a boundary cell such that the method stays stable and formally of second order.

Without loss of generality, the new method of the boundary treatment will be described only for a generalization of the step

$$U_{ij}^{n+\frac{1}{2}} = U_{ij}^n + \frac{\Delta t}{h}(F_{ij}^n - F_{i+1,j}^n) \tag{14}$$

for the boundary cells. Thus we are looking for a method to integrate the equation

$$U_t + F(U)_x = 0 \tag{15}$$

for the boundary cells by a time step Δt.

Consider again the boundary cell C_{ij} on Figure 2. The cell is confined by the boundary segments $\Gamma_1 \cup \Gamma_2 \cup \Gamma_3 \cup \Gamma_4 \cup \Gamma_5$. An integration of equation (15) over the cell C_{ij} yields:

$$\partial_t \int_{C_{ij}} U\, dxdy \ + \int_{\Gamma_2} F\, dy \ + \int_{\Gamma_3} F\, dy \ + \int_{\Gamma_5} F\, dy \ = 0. \tag{16}$$

With equation (16) one obtains a method to integrate equation (15) for the boundary cell C_{ij}, which corresponds to the step (14):

$$U_{ij}^{n+\frac{1}{2}} = U_{ij}^n + \frac{\Delta t}{|C_{ij}|}(F^n(\Gamma_5) \cdot h - F^n(\Gamma_2) \cdot a - F^n(\Gamma_3) \cdot (h - a)). \tag{17}$$

$F^n(\Gamma_j)$, $j = 2,3,5$ are suitable fluxes F along the boundary segments Γ_j, $j = 2,3,5$ to be defined by solving a Riemann problem for equation (15) with initial values

$$U_L(\Gamma_j), U_R(\Gamma_j),\ j = 2,3,5. \tag{18}$$

The exact solution of a Riemann problem for equation (15) consists of shocks, rarefaction waves and contact discontinuities, which travel along the x-axes. To avoid stability problems for the small boundary cells LeVeque has made two suggestions: an enlargement of the domain of dependence [1] and an enlargement of

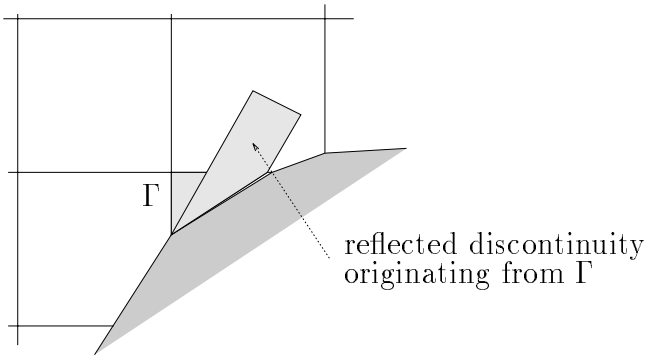

Figure 4: Reflection of a wave at the body boundary.

the domain of influence [9]. By enlarging the domain of influence, the impact of a discontinuity originating from a cell interface gets followed by reflecting the wave at the body boundary (cf. Figure 4).

Our new method to define the fluxes near the boundary (e.g. $F^n(\Gamma_j)$, $j = 2, 3, 5$ in Figure 2) is a combination of [1] und [9]. As discontinuities originating from

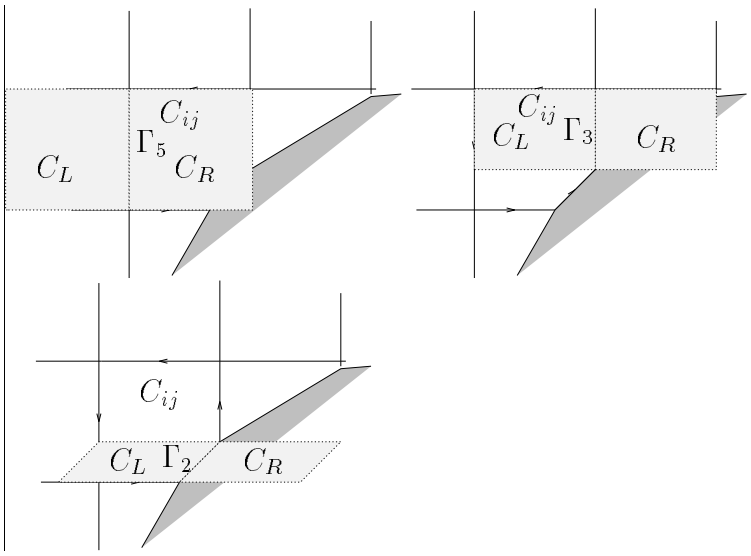

Figure 5: Auxiliary cells for the definition of $U_L(\Gamma_j), U_R(\Gamma_j)$, $j = 2, 3, 5$

the solution of a Riemann problem of equation (15) travel along the x-axes, it makes sense to construct axiliary cells C_L and C_R with a horizontal expansion h for the calculation of the initial values U_L and U_R of the Riemann problems near the boundary (cf. $C_L(\Gamma_j), C_R(\Gamma_j)$, $j = 2, 3, 5$ in Figure 5). The inital values U_X, $X \in$

$\{L, R\}$ are calculated by weighted means with the auxiliary cells C_X, $X \in \{L, R\}$. Two cases are distinguished. In the first case, the auxiliary cell C_X lies totally outside of the body. Then the weighted mean is obtained as follows:

$$U_X = \frac{\sum_{i,j=0}^{N_x-1,N_y-1} U_{ij} \cdot |C_X \cap C_{ij}|}{|C_X|}. \tag{19}$$

$C_X \cap C_{ij}$ is the sectional plane of C_X and C_{ij}. In the other case the auxiliary cell C_X stands into the body across the boundary segment of the boundary cell C_{kl} (In Figure 5 $C_R(\Gamma_2)$ and $C_R(\Gamma_5)$ stand into the body across the boundary segment of the cell C_{ij} and $C_R(\Gamma_3)$ across the boundary segment of the cell $C_{i+1,j}$). This cell C_X gets replaced by two other auxiliary cells C_X^1 and C_X^2. The cell C_X^1 is the part of the cell C_X which lies outside of the body. The cell C_X^2 is obtained by mirroring the part of the cell C_X which lies inside the body at the boundary segment over which it stands into the body (cf. Figure 6). Thus the cells C_X^1 and C_X^2 lie totally outside of the body and it is:

$$|C_X| = |C_X^1| + |C_X^2|. \tag{20}$$

The weighted mean for such an auxiliary cell, which stands into the body across the boundary segment of cell C_{kl}, is then obtained using the operator $R_{kl}(.)$ (cf. equation (7)):

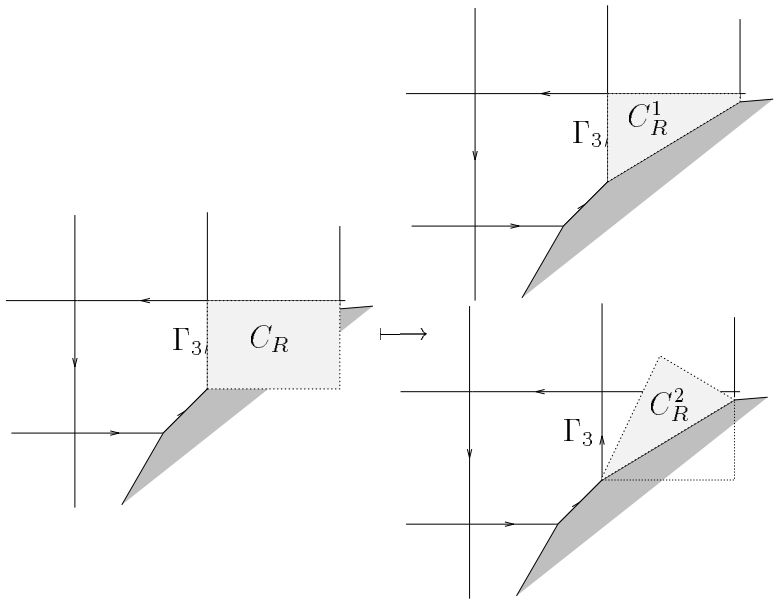

Figure 6: Construction of $C_R^1(\Gamma_3)$ and $C_R^2(\Gamma_3)$ from $C_R(\Gamma_3)$.

$$U_X = \frac{(\sum_{i,j=0}^{N_x-1,N_y-1} U_{ij} \cdot |C_X^1 \cap C_{ij}| + \sum_{i,j=0}^{N_x-1,N_y-1} R_{kl}(U_{ij}) \cdot |C_X^2 \cap C_{ij}|)}{|C_X|}. \tag{21}$$

By this procedure, we get initial values U_L, U_R for every boundary segment Γ to solve a Riemann problem for the equation (15). Solving this Riemann problem, we get a state U^* at the interface Γ and thus a numerical flux $F^n(\Gamma) = F(U^*)$.

3 The Roe solver, second order accuracy and a limiter for the boundary gradients

For a description of the second order accuracy along the boundary, we first describe how to get second order for the regular cells by means of the Roe solver. As already mentioned, to get second order accuracy for a dimensional splitting method, only the fractional steps in (11) have to be of second order. I.e. we are searching for a second order one dimensional method for the step (14).

First we show how to get a second order flux for the cell interface between two regular cells $C_{i-1,j}$ and C_{ij} following [8]. We solve a Riemann problem with initial values $U_L = U_{i-1,j}$ and $U_R = U_{ij}$. To do this approximately by the Roe solver, equation (15) is linearized to [7]:

$$U_t + A(U_L, U_R)U_x = 0,\ A \in \mathbb{R}^{4\times 4}, \tag{22}$$

where of course $A(U,U) = \frac{\partial F}{\partial U}$. To get an upwind method the difference $U_R - U_L$ is decomposed into three vectors, which are eigenvectors of the Roe matrix $A(U_L, U_R)$:

$$U_R - U_L = \sum_{p=1}^{3} \Delta U_p, \text{ where } \quad A(U_L, U_R)\cdot \Delta U_p = \lambda_p \cdot \Delta U_p,\ p = 1,2,3. \tag{23}$$

ΔU_1 and ΔU_3 correspond to shocks and rarefaction waves with characteristic speeds $\lambda_1 = (u-c)(U_L, U_R)$ and $\lambda_3 = (u+c)(U_L, U_R)$ respectively. ΔU_2 corresponds to a contact discontinuity with characteristic speed $\lambda_2 = u(U_L, U_R)$. The upwind flux $F^1(U_L, U_R)$ (in the following, we have suppressed the upper index n for the time step and the lower indices ij for the interface) is then obtained by:

$$F^1(U_L, U_R) = F(U_L) + \sum_{\lambda_p < 0} \lambda_p \cdot \Delta U_p. \tag{24}$$

To fulfil the entropy condition, sonic rarefaction waves get a special treatment (entropy-fix [8] pp. 151-153). E.g. if

$$(u-c)(U_L) < 0 < (u-c)(U_L + \Delta U_1), \tag{25}$$

then the upwind flux $F^1(U_L, U_R)$ is obtained by

$$F^1(U_L, U_R) = F(U_L) + \frac{(u-c)(U_L)\cdot \lambda_1}{(u-c)(U_L + \Delta U_1) - (u-c)(U_L)} \Delta U_1. \tag{26}$$

The flux $F^1(U_L, U_R)$ can be extended to second order by a correction term:

$$F^2(U_L, U_R) = F^1(U_L, U_R) + \frac{1}{2}\sum_{p=1}^{3} |\lambda_p|(1 - \frac{\Delta t}{h}|\lambda_p|)\Delta U_p. \tag{27}$$

In order to avoid oscillations around shocks, one can limit the components of the jumps ΔU_p in the correction term (second part on the right in (27)). Possible limiters are the minmod, the van Leer or the superbee limiter. The superbee limiter lies on the edge of the stability region. The component-wise limitation is done by a limiter factor.

$$(\Delta U_p)_k^{limit} = l_{pk} \cdot (\Delta U_p)_k,\ p = 1, 2, 3;\ k = 1, ..., 4\,(k \text{ indexes } U) \tag{28}$$

The calculation of the limiter factor l_{pk} needs the jumps of the neighboring cell interfaces ΔU_p^{left} and ΔU_p^{right} (known by the calculation of $F^1_{i-1,j}$ and $F^1_{i+1,j}$) and is done by a limiter function $l(.,.)$:

$$l_{pk} = \begin{cases} l((\Delta U_p)_k, (\Delta U_p)_k^{left}) & : \quad \lambda_p > 0 \\ l((\Delta U_p)_k, (\Delta U_p)_k^{right}) & : \quad \lambda_p < 0 \end{cases}, \tag{29}$$

where of the following limiter functions $l(.,.)$ can be used:

$$l(a,b) = \begin{cases} \max(0, \min(1, \frac{b}{a})) & : \text{ minmod limiter} \\ (\frac{b}{a} + |\frac{b}{a}|)/(1 + |\frac{b}{a}|) & : \text{ van Leer limiter} \\ \max(\max(0, \min(1, \frac{2b}{a})), \min(2, \frac{b}{a})) & : \text{ superbee limiter} \end{cases} \tag{30}$$

We mainly use the van Leer limiter.

In case of a flow calculation where no shocks or contact discontinuities appear, there is no limitation of the jump-components of ΔU_p necessary in the second order correction term (e.g. the Prandtl-Meyer expansion in the next section).

The method should also be able to calculate transonic and supersonic flows, where discontinuities in the solution can appear. In order to use the correction term of second order (second term of equation (27)) for such flows, the jumps ΔU_p must be limited also near the boundary. But the jumps ΔU_p^{left} and ΔU_p^{right}, which are needed for the limitation, are not available yet for some fluxes near the boundary after the calculation of the first order flux $F^1(U_L, U_R)$ (unlike for the interior fluxes where by means of the calculation of $F^1_{i-1,j}$ and $F^1_{i+1,j}$ the jumps ΔU_p^{left} and ΔU_p^{right} are known). Thus to limit the jumps ΔU_p close to the boundary with ΔU_p^{left} and ΔU_p^{right}, we have to solve some additional Riemann problems along line segments Γ^{left} and Γ^{right} (cf. Figure 7 for the fluxes $F^n(\Gamma_j)$, $j = 2, 3, 5$ of the boundary cell C_{ij} of figure 2). To solve a Riemann problem along such a line segment Γ, which can also be lying beyond the boundary of the body, we construct again auxiliary cells $C_L(\Gamma)$ and $C_R(\Gamma)$ like in the previous section. To get the initial states of the Riemann problem $U_L(\Gamma)$ and $U_R(\Gamma)$, we calculate again weighted means. If an auxiliary cell lies partly or totally beyond the boundary, again a mirroring procedure is necessary

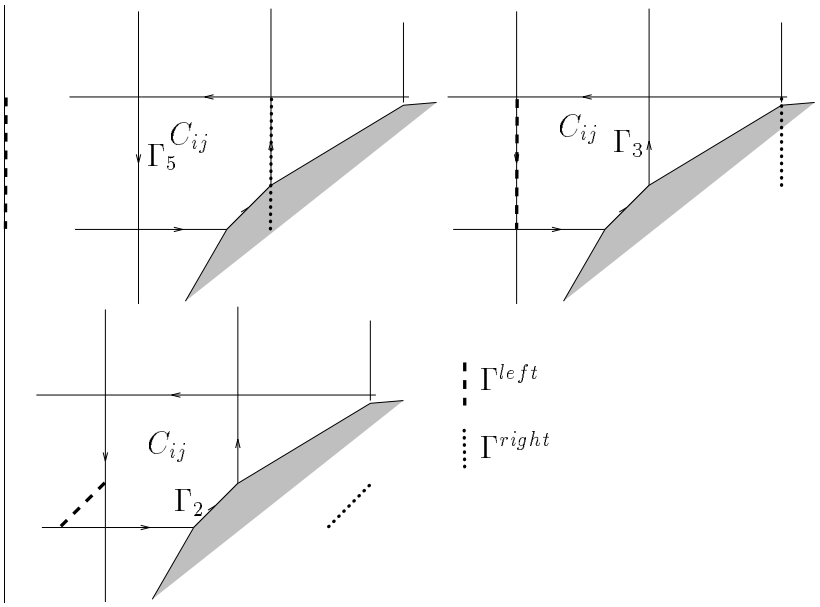

Figure 7: Γ^{left} and Γ^{right}, along which the jumps ΔU_p are needed for the limiting.

at the boundary segment, over which the cell stands horizontally into the body (cf. previous section).

The method is formally of second order accuracy. But as long as piecewise constant reconstructions are used for the calculations of the weighted means over the auxiliary cells, it is not sure if the actual value for the order will reach a value of 2.0. But certainly it will be higher than 1.0.

4 Numerical results

For the Prandtl-Meyer expansion of a 1.2 Mach flow over a 30^0 bend, the exact solution is smooth (cf. numerical solution with a grid parameter $h = \frac{1}{80}$ in Figure 8). Therefore the calcultation can be done without limiting the jumps in (27), provided that the initial flow field is sufficiently close to the exact solution. Such an initial flow can be obtained by sending a shock over the bend with the limiter turned on whose left hand side is a Mach 1.2 flow and whose right hand side is a flow at rest. For the exact solution, entropy and stagnation enthalpy are constant thus are known. Therefore we can easily do an error analysis (cf. [1] [3]). Comparing entropy and stagnation enthalpy of the numerical solution for a grid parameter h with the corresponding value of the exact solution, we can calculate the error in the

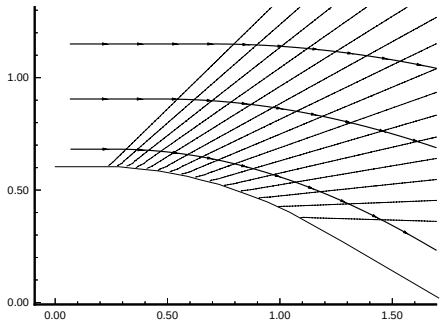

Figure 8: 30^0 Prandtl-Meyer expansion of a Mach 1.2 flow (density contours and stream lines).

L_1-norm in the whole flow area or only along the boundary of the body:

$$error_{total} = \frac{\sum^1 |u_{ij} - u^c_{ij}|}{\sum^1 |C_{ij}|}, \tag{31}$$

$$error_{boundary} = \frac{\sum^2 |u_{ij} - u^c_{ij}|}{\sum^2 |C_{ij}|}, \tag{32}$$

where u^c_{ij} is the exact solution (here entropy or stagnation enthalpy), u_{ij} is the numerical solution, $\sum^1$ is a summation over all the grid cells, and $\sum^2$ is a summation over the boundary cells only.

Under the assumption that the error can be expressed as $error = C \cdot h^p$, we can calculate the order p of the method in the whole area or only along the boundary (cf. Table 1).

As in [3], the results for entropy suggest that the method is of second order accuracy in the whole area. But the value of $p = 1.4$ for the order in entropy along the boundary is an improvement comparing with other Cartesian grid methods. The results for stagnation enthalpy are less satisfying, as in [3] as well.

The double Mach reflection [10] is an attractive numerical experiment for a supersonic flow, especially for a test of the boundary treatment. The flow phenomenona of a double Mach reflection arise by reflecting a shock which is strong enough at a ramp (cf. Figure 9). At the origin of the ramp a self similar structure arises with two Mach stems. The contact discontinuity of the second stem is very weak. Also the reflected shock of the second stem is very weak and disappears where it encounters the contact discontinuity of the first stem. There the fluid gets dense, so that a jet forms which moves towards the reflected shock of the first stem. The width of this jet is sensitive to the boundary treatment.

The orientation of the grid was chosen such that the orthogonal axes is aligned

h	entropy		stagnation enthalpy	
	$error_{total}$	order	$error_{total}$	order
$\frac{1}{160}$	0.0000680	-	0.001138	-
$\frac{1}{320}$	0.0000184	1.89	0.000637	1.11
$\frac{1}{340}$	0.0000164	1.90	0.000597	1.07
	$error_{boundary}$		$error_{boundary}$	
$\frac{1}{160}$	0.001114	-	0.0172	-
$\frac{1}{320}$	0.000441	1.34	0.0122	0.50
$\frac{1}{340}$	0.000405	1.40	0.0118	0.55

Table 1: Convergence history for the Prandtl-Meyer expansion.

with the moving shock. The angle of the ramp and the moving shock was 60^0. The ramp and the lower edge are solid wall boundaries. For the outflow boundaries on the right hand side and the upper edge, we have chosen a supersonic outflow boundary condition.

In a comparison of the boundary treatment with or without the second order correction term (27) in the fluxes along the boundary (cf. Figure 10), the smearing of the reflected shock of the first stem along the boundary could almost be avoided with the second order accurate boundary treatment. The jet in the direction of the main reflected shock along the boundary is narrower with the second order boundary treatment.

The double Mach reflection is an unsteady problem. As an other steady problem, we have chosen a transonic flow past a bump [11]. A subsonic Mach 0.85 gas flows past a bump whose width is 5% of its length. In this case we have to impose subsonic boundary conditions on the inflow, the outflow and the upper edge. Along the lower edge, we have a wall boundary. For the subsonic boundary condition, we have chosen an algorithm found in [12]. I.e. the initial values U_L for the Riemann problems along the interfaces on the left domain boundary are obtained by imposing stagnation enthalpy and entropy and by the fact that one wave leaves the domain leftwards. The initial values U_R for the Riemann problems along the interfaces on the right domain boundary are obtained by imposing free pressure and by the fact that two waves leave the domain rightwards. On the upper domain boundary, the sign of the orthogonal velocity component determines, if we have to impose an inflow or an outflow boundary condition.

The exact solution of a flow over the bump is subsonic, symmetric and isentropic for Mach numbers $<\sim 0.75$. For an inflow Mach number of 0.85 (cf. Figure 11), the flow on the back of the bump exceeds the speed of sound and gets subsonic again

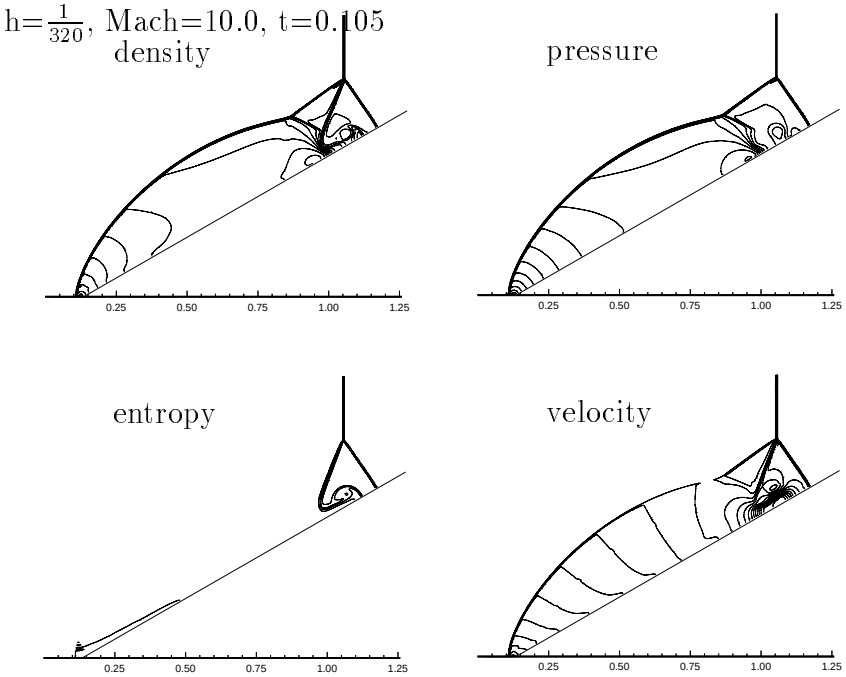

Figure 9: Double Mach reflection, calculated with a 400x320 grid.

by a steady shock wave.

On Figure 12 we plotted the entropy along the back of the bump for a calculation with a first and a second order boundary treatment. The entropy production is physical only at the location of the shock. The comparision shows that the numerical entropy production at the beginning and the end of the bump is less and sharper with the second order boundary treatment.

As one of the main advantages of the use of a Cartesian Grid method, one can calculate flows around complicated geometries without too much effort in the grid generation. In addition the simple data structure makes it possible to write fast computer codes.

Already a flow past two cylinders would be rather complicated with body fitted or adaptive grids. To illustrate this, we calculate the reflection phenomena of a shock with relative Mach number 2.31 passing two cylinders which are shifted with respect to each other. This example was also calculated in [1]. For the calculation we used a 400x400. The second dimension seems to be rather big, but so we could minimize spurious reflections of the shocks at the upper and the lower domain boundary. Figure 13 shows a contour plot of the solution at a time t=0.22. The initial shock location at t=0.0 is just in front of the lower cylinder. We can see the rise of an interesting structure with two shocks hitting the lower cylinder. The pressure plot

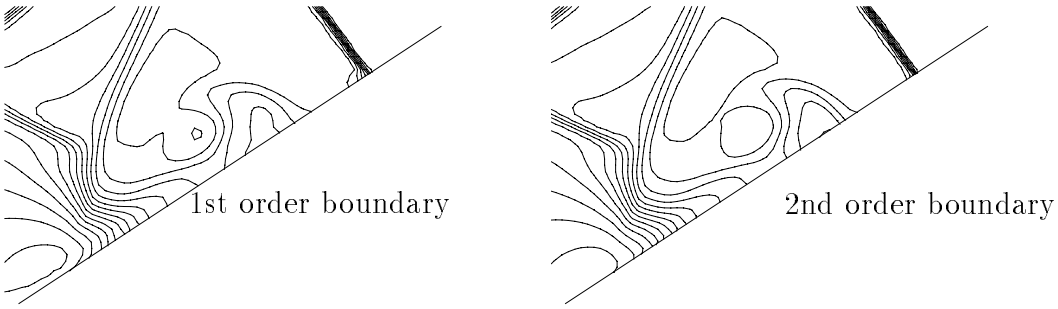

Figure 10: Density contours for the double Mach reflection (detail of a 300x250 grid). Comparision of a first and second oder boundary treatment.

on Figure 14 shows the two shocks incident on the lower cylinder, just above the pressure peak at the leading edge. Due to the second order boundary treatment, they are well resolved.

5 Conclusions

A new method was presented for the treatment of the small boundary grid cells, which arise along a body using a Cartesian grid. We used a dimensional splitted finite volume method to simulate the unsteady, inviscid, compressible flow around an

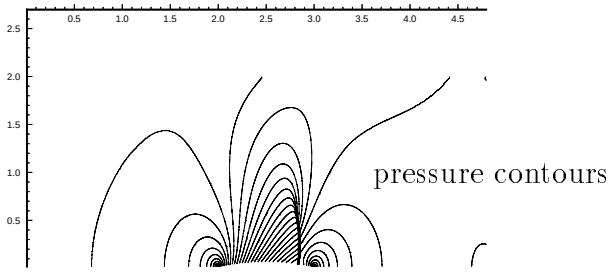

Figure 11: Mach 0.85 flow past a 5% bump for a grid parameter $h = 0.01$.

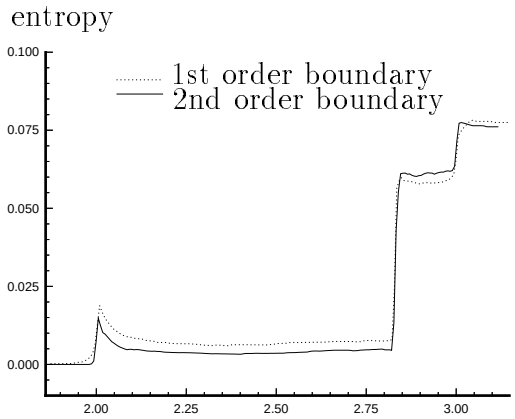

Figure 12: Flow past a circular bump. Comparison of a calculation with first and second order boundary treatment.

arbitrary body in two space dimensions. The method was built upon a dimensional splitted standard method because of simpler coding but also because of simpler data structure which results in a high speed executable program. In a first step, we have constructed a stable method which was of first order accuracy along the boundary of some body. This method was extended to second order accuracy also along the body boundary, which made it necessary to build a limiter of the gradients for the boundary cells. By means of a smooth steady flow, we measured the order of the algorithm in the whole domain and along the boundary. Along the boundary we got an order of 1.4 which is an improvement comparing with other boundary treatments. We also calculated the unsteady double Mach reflection, where we showed that a second order boundary treatment is necessary to avoid smearing of unsteady shocks wandering along the boundary. Also the numerical entropy production along the boundary cells is lower for a boundary treatment of second order.

In a next step we have made the method conservation preserving. To do this, we summed up for one time step in each boundary cell the errors the method makes in mass and energy conservation and in momentum transfer from the body not coming from pressure. Then we distribute these errors as a correction term among the neighboring cells without disturbing the order of the method. This additional step is similar as the second step of the method [3] described in the introduction. The results in order as well as accuracy did not change noticeably.

An important feature of the method is its simplicity. This fact be useful for an extension of the method to calculate flows in three space dimensions, which is a possible continuation of this work. An other possible direction to go would be to generalize the new boundary treatment to other non dimensional splitted methods, e.g. the method of transport [13].

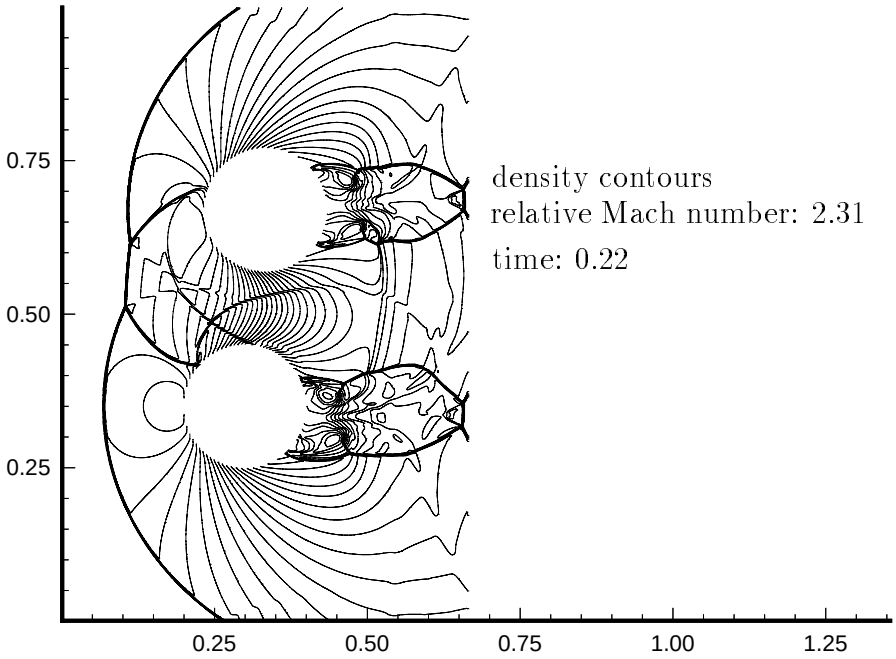

Figure 13: Reflection of a shock traveling at Mach 2.31 off two cylinders with a grid parameter $h = 0.0025$.

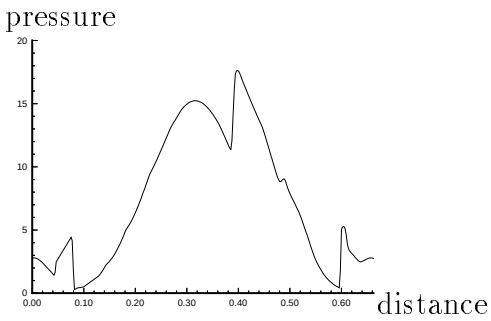

Figure 14: Pressure along the lower cylinder at t=0.22.

References

[1] R.J. LeVeque M.J. Berger. *A Rotated Difference Scheme for Cartesian Grids in Complex Geometries.* AIAA Paper CP-91-1602, 1991.

[2] R.J. LeVeque M.J. Berger. *Stable Boundary Conditions for Cartesian Grid Calculations.* ICASE Report No. 90-37, May, 1990.

[3] P. Colella W.Y. Crutchfield M.L. Welcome R.B. Pember, J.B. Bell. *An Adaptive Cartesian Grid Method for Unsteady Compressible Flow in Irregular Regions.* Journal of Comp. Phys., 120, pp 278-304, 1995.

[4] J.J Quirk. *An alternative to unstructered grids for computing gas dynamic flows around arbitrarily complex two-dimensional bodies.* Computers Fluids, Vol. 23 No. 1, pp 125-142, 1994.

[5] P. Colella M.J. Berger. *Local Adaptive Mesh Refinement for Shock Hydrodynamics.* J. Comp. Phys. , Vol. 85, 1989.

[6] G. Strang. *On the construction and comparison of difference schemes.* SIAM J. Num. Anal., 5, pp. 506-517, 1968.

[7] P.L. Roe. *Approximate Riemann Solvers, Parameter Vectors, and Difference Schemes.* J. Speed Computing, Vol.4. No.1, 1992.

[8] R.J. LeVeque. *Numerical Methods for Conservation Laws.* Birkhäuser Verlag, 1992, ETH Zürich.

[9] R.J. LeVeque. *High Resolution Finite Volume Methods on Arbitrary Grids via Wave Propagation.* Journal of Comp. Phys., 78, pp. 36-63, 1988.

[10] P. Colella P. Woodward. *The Numerical Simulation of 2D Fluid Flow with Strong Shocks.* J. Comp. Phys. , Vol. 54, pp 115-173, 1984.

[11] J. Chan S. Liang. *An Improved Upwind Scheme for the Euler Equations.* J. Comp. Phys., Vol. 84, pp. 461-473, 1989.

[12] N. Botta. *Numerical investigation of 2D Euler flows.* Dissertation ETH No. 10852 am Seminar f"ur angewandte Mathematik, 1994.

[13] M. Fey. *Ein echt mehrdimensionales Verfahren zur Lösung der Eulergleichungen.* Dissertation ETH No. 10034 am Seminar für angewandte Mathematik, 1993.